JOURNAL OF MODERN OPTICS, 1998, VOL. 45, NO. 2, 227–237

Annular binary filters for controlling the axial behaviour of optical systems

TOMASZ CICHOCKI, MANUEL MARTÍNEZ-CORRAL
Departmento de Optica, Universidad de Valencia, 46100 Burjassot, Spain

MAREK KOWALCZYK
Institute of Geophysics, Warsaw University, Pasteura 7, 02-093 Warsaw, Poland

and PEDRO ANDRÉS
Departamento de Optica, Universidad de Valencia, 46100 Burjassot, Spain

(*Received 5 December 1996; revision received 6 June 1997*)

Abstract. The one-dimensional (1D) version of the iterative Fourier transform algorithm (IFTA) and a modified error diffusion algorithm are proposed for binarizing rotationally symmetric pupil filters designed to shape the axial impulse response of optical system. The resulting binary masks consist of a set of transparent and opaque annular zones of equal area or equal width. A numerical experiment in which we examine the performance of the binarization methods is carried out. In this experiment the resemblance between the axial diffractive behaviour of the binary version of an axially superresolving pupil filter, and that of the original continuous-tone filter is evaluated. It is shown that the performance of the binary mask obtained with 1D IFTA is much better than that of the annular binary filters obtained by other digital half-toning techniques which preserve the rotational symmetry of binarized pupils.

1. Introduction

In many optical devices, for example in confocal scanning microscopes, the axial amplitude distribution in the image of a point source, that is the axial amplitude impulse response (AAIR) of the optical system, is a matter of interest. Therefore several efforts have been addressed to control this characteristic. As the axial response of a pupil filter is determined by its radially averaged transmittance, certain radially symmetric pupil filters have been proposed to shape this response on purpose. As some examples we can mention pupils which yield high focal depth [1, 2], reduction of the influence of spherical aberration [3], axial superresolution [4, 5] and improvement in the optical sectioning capacity in confocal scanning microscopy [6, 7]. On the other hand, the manufacture of pupil filters in which the amplitude transmittance is a continuous function of the radial coordinate is a difficult task. In the case of real non-negative pupil functions (purely absorbing filters) a possible method to overcome this difficulty is to replace them by binary functions obtained by means of digital half-toning. Filters whose transmittance is complex have to be coded as holograms, for example binary Gabor holograms [8]. Both classes of binary elements can be easily produced by light plotters or laser printers.

A variety of half-toning algorithms designed for binarization of continuous-tone pictures or for computer generation of binary diffractive optical elements have been already reported [9]. When these methods are used, the spatial frequency spectrum of a binary object becomes a sum of a binarization-noise spectrum and the spectrum of the original continuous-tone object. Recently some half-toning techniques for binarizing grey-tone pupil filters with the aim of obtaining a high resemblance between the transverse intensity impulse response (TIIR) of the binary mask and that of the original pupil filter have been proposed [10, 11]. As digital half-toning techniques are usually based on two-dimensional (2D) regular grids (rectangular or hexagonal), this leads in the case of binarized rotationally symmetric pupil filters to an additional deformation of TIIR: the rotational symmetry of the original TIIR is broken.

A solution to this problem can be found by means of one-dimensional (1D) binarization methods processed along the radius of the pupil. There are methods which yield rotationally symmetrical binary filters reported in the literature. Hegedus [12] proposed three methods for such filters. They are based on pupil subdivision into annuli of equal width, into annuli of equal area or into annular zones with adapted width. These methods require, in principle, arbitrary high resolution of the printing device, as the transmitting part of each annulus has to transmit the same amount of energy as the corresponding zone in the continuous filter. Thus such filters are hardly printable by the devices which offer not very high resolution.

Recently Kowalczyk *et al* [13] proposed two methods based on the adapted error diffusion (ED) technique. The resulting binary filters, depending on the method, consist of sets of transparent and opaque annular zones of equal width or equal area. The number of the zones depends only on the resolution of the printing device and the size of the pupil and is set before the binarization process. In spite of the fact that these methods were designed for Fourier plane response, they can also be used for shaping the axial response.

For implementation of rotationally symmetric binary mask that shapes the AIIR, Rosen and Yariv [14] proposed the use of a direct binary search (DBS) algorithm for coding a phase-only radially symmetric distribution in a binary computer-generated hologram. This method has two drawbacks. On the one hand, the use of a DBS algorithm starting from a random binary filter reaches a local minimum of the reconstruction error very quickly. On the other hand, owing to the holographic coding, the obtained axial intensity response is periodic (higher-order foci), which is quite far from the aim of this work.

In this paper we propose the use of a 1D iterative Fourier transform algorithm (IFTA) [15] and 1D modifications of ED. The use of the IFTA is justified by the fact that the AIIR of a rotationally symmetric filter can be easily evaluated by the 1D Fourier transform of the properly mapped transmittance profile of the filter [16]. Similarly the filter profile needed for a certain axial impulse response can be obtained by the inverse transform. Thus to binarize the amplitude transmittance of the filter it seems that the 1D IFTA is an adequate tool. The use of this algorithm allows one to obtain the AIIR of a binary filter virtually identical with the response of a continuous filter within a specified region.

As the ED technique has been up to now considered for focal plane applications, the axial properties of this algorithm have, in fact, already been determined. This is because the equal-area-zone (EAZ) ED algorithm [13] is a version of a well known 1D ED algorithm supporting an error-free region centred at the origin of the spectral domain [17]. This means that these already-proposed methods can be used for the task of binarizing axial apodizers.

In a numerical experiment the performance of a binary mask obtained by means of IFTA is evaluated in terms of the signal-to-noise ratio (SNR) for the case of an axially superresolving purely absorbing pupil filter. Then a similar evaluation is performed for the filters generated with algorithms based on 1D ED. The axial diffractional behaviour of the IFTA filter is found to be much better than those generated by other algorithms.

2. Axial amplitude impulse response of pupil filters

Let us start by considering the AAIR of an aberration-free imaging system that is apodized by a radially symmetric pupil function $p(r)$, that is [16]

$$u(z) = 2\int_0^{r_0} p(r)\exp\left[-\,\mathrm{i}2\pi\frac{z r_0^2}{2\lambda f(f+z)}\left(\frac{r}{r_0}\right)^2\right] r\,\mathrm{d}r, \tag{1}$$

where r_0 represents the maximum radial extent of the pupil filter, z is the axial coordinate measured from the image plane and f is the focal length of the system, as depicted in figure 1.

It is apparent that the integral relation of equation (1) can be easily converted into a 1D Fourier transformation. To this end we propose the following geometrical mapping:

$$\zeta = \frac{r^2}{r_0^2} - 0{\cdot}5, \quad q(\zeta) = p[r(\zeta)]. \tag{2}$$

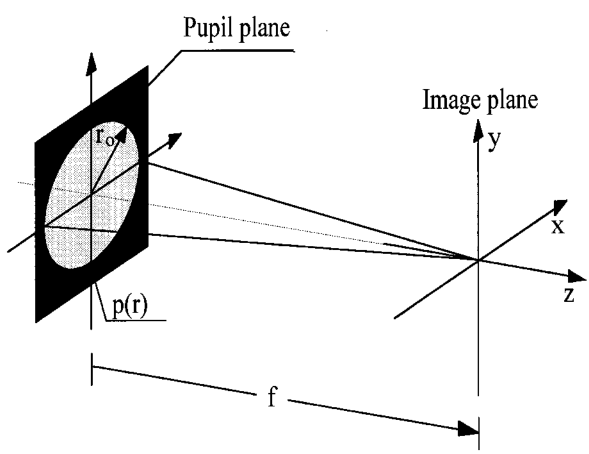

Figure 1. Schematic representation of the optical set-up under consideration.

Then, equation (1) can be rewritten, apart from irrelevant phase and constant factors, as

$$u(z) = \int_{-0\cdot5}^{0\cdot5} q(\zeta) \exp\left(-\mathrm{i}2\pi \frac{Nz}{2(f+z)}\zeta\right) \mathrm{d}\zeta, \tag{3}$$

where the parameter $N = r_0^2/\lambda f$ represents the Fresnel number of the pupil, that is the number of Fresnel zones that are covered by the pupil as viewed from the axial point of the image plane, $z = 0$.

Equation (3) states that the AAIR of an optical system is governed by the 1D Fourier transform of the mapped version of the amplitude transmittance $q(\zeta)$ of the pupil filter. The Fourier transform is calculated for an axial spatial frequency $Nz/2(f+z)$ which is nonlinear with respect to z and is equal to the well known defocus coefficient W_{20}

$$W_{20} = \frac{Nz}{2(f+z)}. \tag{4}$$

Now, by substituting equation (4) into equation (3) we obtain

$$u(z) = Q(W_{20}) = \int_{-0\cdot5}^{0\cdot5} q(\zeta) \exp(-\mathrm{i}2\pi W_{20}\zeta)\, \mathrm{d}\zeta \tag{5}$$

3. Binarization of the function $q(\zeta)$

As established in section 2, the AAIR of a radially symmetric apodized imaging systems is proportional to the 1D Fourier transform of the function $q(\zeta)$. It is then apparent that, if we are interested in obtaining a binary mask which reproduces the axial response of pupil filters designed to control the AIIR of an optical system, it is precisely $q(\zeta)$ the function which should be binarized. Furthermore, to reach this aim an algorithm specially designed for obtaining strong resemblance between the low-frequency spectra of the binary mask and its continuous-tone counterpart should be used. Then, the 1D version of the IFTA and ED are the adequate binarization techniques.

The IFTA originates from the phase retrieval problem [18]. Using this algorithm, one searches iteratively for a pair of functions fulfilling simultaneously a set of constraints in both Fourier and space domains. The original algorithm was aimed at finding an object from modulus of its Fourier transform. In diffractive optics, IFTA allows one to obtain a binary mask whose Fourier transform is in certain regions of the spatial frequency domain virtually identical with the Fourier transform of a continuous-tone filter [15]. The flow chart of the IFTA is presented in figure 2.

The operators used in the algorithm are defined as follows:

$$U^{(k)} q_j(\zeta) = \begin{cases} 0, & |q_j(\zeta)| \leqslant e^{(k)}, \\ 1, & |q_j(\zeta)| > 1 - e^{(k)}, \\ |q_j(\zeta)|, & \text{otherwise}, \end{cases} \tag{6}$$

and

$$H\tilde{Q}_j(W_{20}) = \begin{cases} \beta_j |Q(W_{20})| \exp\{\mathrm{i} \arg[\tilde{Q}_j(W_{20})]\}, & W_{20} \in S, \\ Q_j(W_{20}), & \text{otherwise}. \end{cases} \tag{7}$$

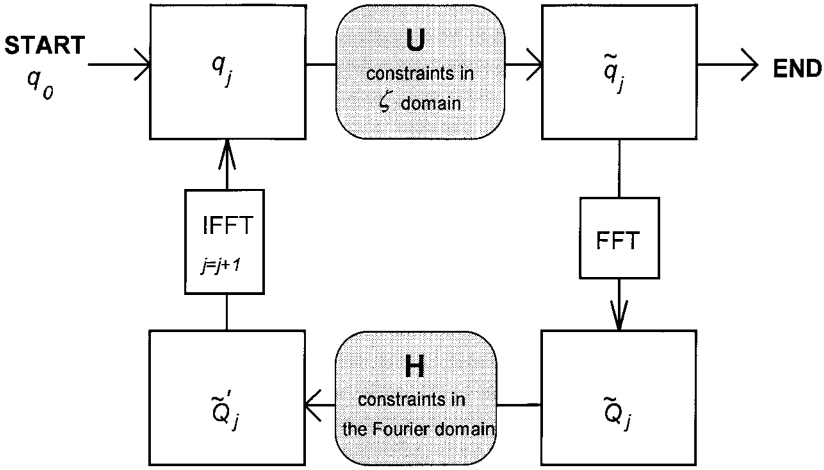

Figure 2. The flow chart of IFTA.

The algorithm starts with sampling the mapped transmittance in M equidistant points $\zeta_i = (2i - M + 1)/2M$, where $i = 0, \ldots, M - 1$. Then, the discrete function undergoes a nonlinear transform by operator U, which represents constraints in the ζ domain. The modified function $\tilde{q}(\zeta_i) = Uq(\zeta_i)$ is Fourier transformed (usually by a fast Fourier transform (FFT)) and the function $\tilde{Q}(W_{20})$ is obtained. Now, Fourier domain constraints H are imposed. After this modification the function is inversely transformed to the ζ domain and U is again applied on it.

The operator U is a tunable nonlinear function which allows one to avoid the stagnation of the binarization process [15]. The parameter $e^{(k)} \in]0, 0{\cdot}5]$ is increased after a specified number of iterations. Finally U approaches the thresholding operator. Thus final loops of the iteration process are executed with the hardclip ($e^{(k)} = 0{\cdot}5$). The operator H represents constraints in the Fourier domain. In the region S it substitutes the modulus of the spectrum of modified function by the modulus of the spectrum of original continuous-tone function. The proportionality coefficient β_j, which minimizes the quadratic deviation of $|\tilde{Q}_j|$ from $|Q|$ over the window S, is calculated in each iteration. When the procedure is terminated, the inverse mapping of $\tilde{q}_j(\zeta_i)$ into the r domain leads to the actual filter consisting of a set of M concentric annular zones of equal area. This configuration of the filter will be referred to as an EAZ filter.

An alternative method for attempting to binarize axial apodizers is to use the 1D version of the error diffusion algorithm [19]. Kowalczyk *et al.* [13] have already proposed the use of such algorithm with the aim of obtaining binary masks that reproduce the transverse behaviour of radially symmetric pupil filters. They proposed two methods of pupil subdivision.

In the first method the area of the pupil is divided into annular equal-width zones (EWZs), which implies that one should apply the ED algorithm to the function $p(r)$ and not to $q(\zeta)$. Therefore the radius r_0 should be divided into N intervals of equal length. With this division each zone has a different area. We take this into account by proper weighting of the error to be diffused from one zone to the next. The weighting factor $w(i)$ must be equal to the ratio of the area $D(i - 1)$

of the already-binarized zone to the area $D(i)$ of the zone under binarization. With the inner radius of the ith annular zone equal to ir_0/N, we have that

$$w(i) = \frac{D(i-1)}{D(i)} = \frac{2i-1}{2i+1}, \quad i = 0, \dots, N-1. \tag{8}$$

A second fact to be considered is that the direction of the binarization process clearly affects the quality of the resulting binary filter. If the procedure is executed starting with $i = 0$, that is from the centre of the filter, the error obtained at the last sample, which indeed has the largest area, remains uncorrected. In order to minimize the uncorrected error the algorithm should be processed in the opposite direction, that is starting from $i = N - 1$. In this case the diffusion weight applied is

$$w'(i) = \frac{D(i+1)}{D(i)} = \frac{1}{w(i+1)}. \tag{9}$$

In the second method the area of the pupil is divided into concentric annular zones of equal area, what implies that one should apply the ED algorithm to the function $q(\zeta)$. This is because the annuli of equal area in the pupil correspond now to the intervals of the equal length in the ζ domain. Consequently, the weighting factor becomes constant and equal to unity.

4. Numerical experiment

The viability of the methods proposed in Section 3 was established in a numerical experiment. We considered a filter function $p(r) = (2r^2 - 1)^2$, $r \in [0, 1]$ (figure 3 (a), broken curve), which exhibits superresolving properties along the optical axis [20]. After the mapping described in equation (2), $p(r)$ takes the form of parabolic function $q(\zeta) = 4\zeta^2$, $\zeta \in [-0{\cdot}5, 0{\cdot}5]$ (figure 3 (b), broken curve). We aimed to get a binary filter supporting an AIIR virtually identical with that of a continuous filter within the interval A which is centred about the focal point and is bounded by the second-order minima of AIIR. We evaluated the results of our simulation using the SNR defined as

$$\mathrm{SNR}(M) = \left(\int_A |Q(W_{20})|^4 \,\mathrm{d}W_{20} \right) \Big/ \left(\int_A \left[|Q(W_{20})|^2 - \alpha(M) |B(W_{20}; M)|^2 \right]^2 \mathrm{d}W_{20} \right), \tag{10}$$

where the coefficient

$$\alpha(M) = \left(\int_A |Q(W_{20})|^2 |B(W_{20}; M)|^2 \,\mathrm{d}W_{20} \right) \Big/ \left(\int_A |B(W_{20}; M)|^4 \,\mathrm{d}W_{20} \right) \tag{11}$$

maximizes the SNR, $B(W_{20}; M)$ being the AAIR of the resulting binary mask. This SNR is a measure of the resemblance between corresponding AIIRs and, in general, depends on the selected number M of binary zones [13].

The AIIRs of binary filters were calculated as the squared modulus of coherently added Fourier transforms of all transparent binary cells, that is sincus functions multiplied by corresponding phase factors. Thus the integrations of equations (10) and (11) were performed on continuous functions.

Three following binarization algorithms were applied on $p(r)$. First we binarized it by the proposed 1D IFTA procedure. To this end the function $q(\zeta)$ was sampled in $M = 20$ equally spaced points ζ_i. In order to obtain a sufficiently dense

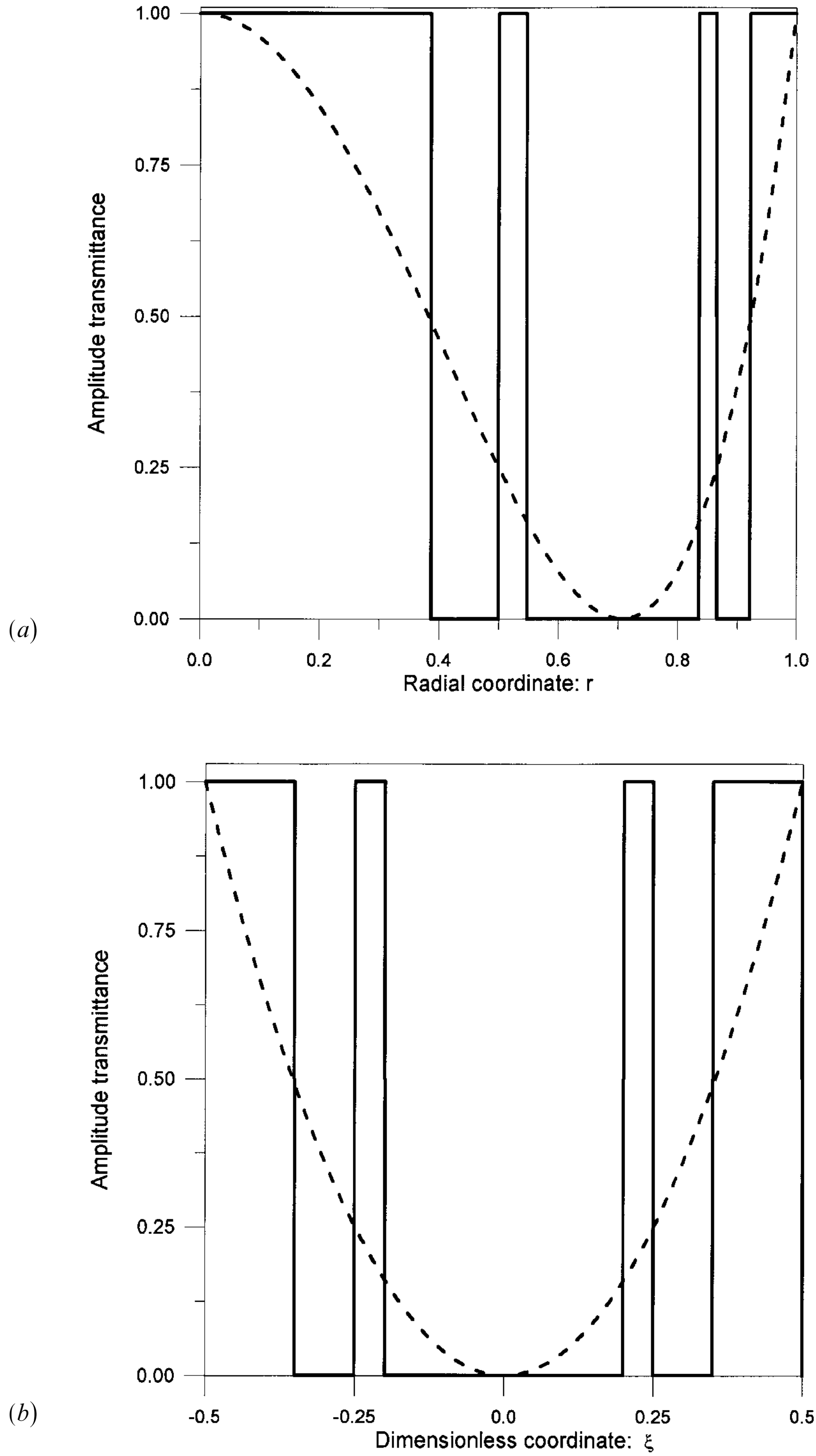

Figure 3. Binary version of axially superresolving pupil filter obtained by the 1D IFTA method for $M = 20$: (*a*) representation in the r domain; (*b*) representation in ζ space. The broken curves represent the amplitude transmitance of the continuous-tone filter.

sampling within the interval S, the function $q(\zeta)$ was surrounded by zeros and formed the vector of 140 pixels. When the Fourier transform is calculated by means of a FFT, this is the usual way used to control the density of sampling in the spectral domain (for example [17]). The vector obtained in this way served as an input for the IFTA algorithm. The parameter $e^{(k)}$ (equation (6)) was increased from 0·05 to 0·5 by 0·05; therefore $k = 1, 2, 3, \ldots, 46$. The free parameters in this case were the number of iterations between the changes from $e^{(k)}$ to $e^{(k+1)}$ in the nonlinear operator U, and the extension of the spectral region S in which we exchange the spectra in the successive loops of the algorithm as, in principle, the areas A and S need not coincide. We found that the reasonable number of iterations after which $e^{(k)}$ should be increased equals three. A further increase in the number of iterations did not influence the result and increased the computation time only. During the experiment we also revealed that the size of spectral exchange region S influences the SNR. This made us look for an optimal region S in which the moduli of the corresponding spectra were replaced (equation (7)). We found that S consisting of 40 central samples maximizes the SNR, that is we found optimal S to be slightly wider than A.

The amplitude transmittance of the binary filter obtained by the iterative technique is presented in figure 3. The solid lines in figures 3 (*a*) and (*b*) represent the binary filter in the r and ζ domains respectively. The negative of the actual filter is presented in figure 4 (*a*). The SNR calculated for this filter is equal to

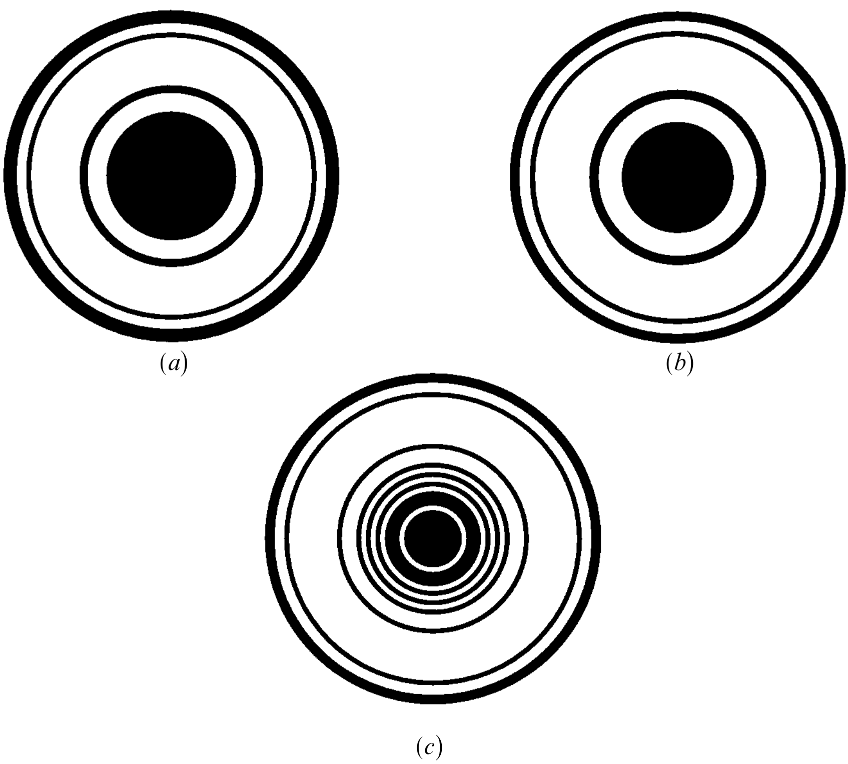

Figure 4. (*a*) The negative of the actual filter consisting of 20 EAZs obtaining by IFTA; (*b*) the negative of the ED filter consisting of 18 EAZs; (*c*) the negative of the ED filter consisting of 35 EWZs.

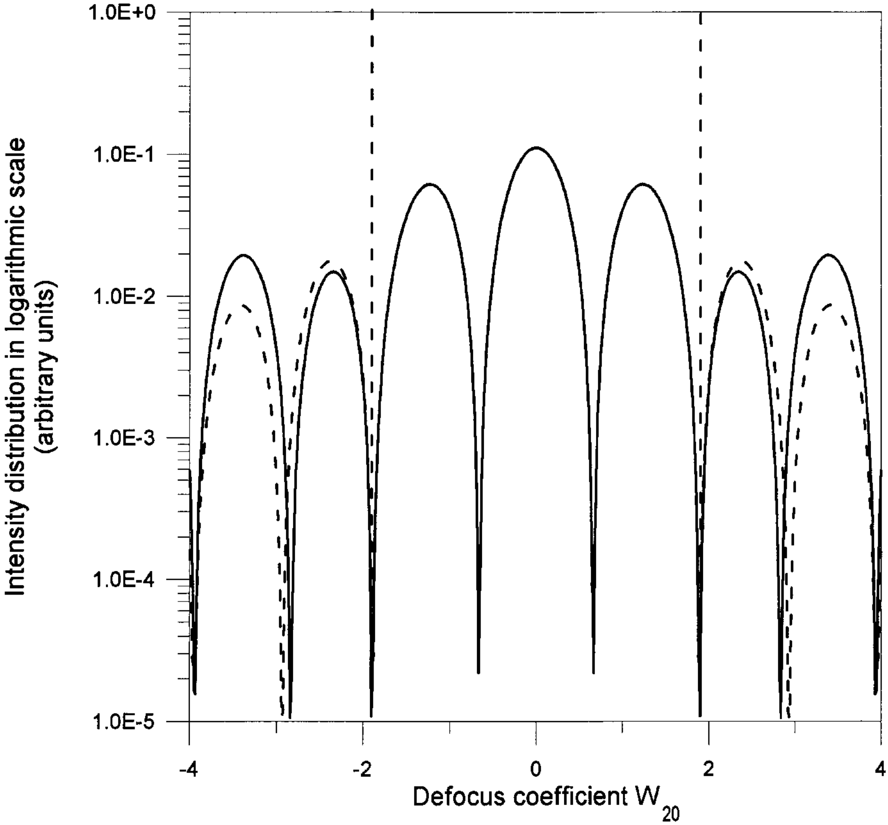

Figure 5. The AIIRs of the binary IFTA filter (———) and original grey-tone filter (- - - - - -). The SNR was calculated in the region between the two vertical broken lines. The AIIR of the binary filter was multiplied by $\alpha(M)$.

46 167. This high value is justified as within the window A the distribution $\alpha(M)|B(W_{20}, M)|^2$ coincides almost perfectly with $|Q(W_{20})|^2$ (figure 5). The parameter $\alpha(M)$ (equation (11)) is equal to 0·70 for the binary filter. Its inverse, $\alpha^{-1}(M)$, can be considered a light efficiency of the binary pupil filter related to the light efficiency of the underlying grey-tone filter. In our case the light efficiency of continuous filter is about 30% less than the light efficiency of its binary counterpart.

Then the binary filter obtained by the IFTA technique was compared with binary filters obtained with the ED algorithm. Before presenting the results, two important facts, which were pointed out in [13], have to be commented on. First, the SNR is not a monotonic function of the number of EAZs or EWZs. There exists some privileged numbers of zones for which SNR is considerably higher than for a slightly smaller or a slightly larger number of zones. Therefore the requirement of spatial resolution as high as possible does not always maximize the SNR. This means that, if it is possible to print a filter consisting of M annular EAZs, one has to evaluate also the performance of filters which are composed of less than M zones to find the best. The second problem deals with the comparison

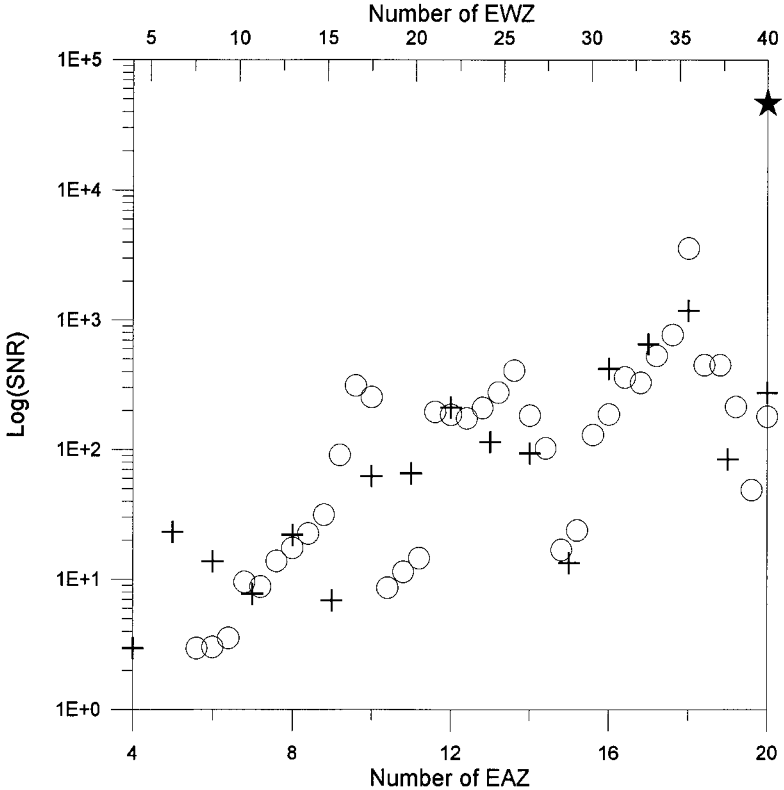

Figure 6. The comparison of SNRs obtained with EAZ (+) and EWZ (○) ED filters; (★), SNR of the IFTA filter consisting of 20 EAZs.

of EAZ and EWZ algorithms. If the printing device has the same resolution for both kinds of annular filter and is able to produce an EWZ filter with N zones, it will produce an EAZ filter consisting of $M = N^2/(2N - 1)$ zones only. Thus the performance of an EAZ filter consisting of 20 annuli should be compared with the performance of an EWZ filter consisting of up to 40 zones.

The combined plot of these two cases is presented in figure 6. The filters produced by the ED technique demonstrate the highest SNR for 18 EAZs and 35 EWZs. Their SNRs equal 1183 and 3575 respectively. The negatives of the EAZ and EWZ filters are presented in figures 4 (*b*) and (*c*) respectively. Note that SNRs obtained with both ED techniques are lower than the SNR of an IFTA filter by one order of magnitude.

We have also calculated the intensity impulse response of the filters in the focal plane for all of the three cases. Their SNRs were calculated according to equations (10) and (11) after the necessary modifications. In this case the SNR obtained for the IFTA filter was also higher than the SNRs of ED filters by one order of magnitude.

5. Conclusions

In this paper the 1D IFTA and modified 1D ED algorithms are applied to produce binary filters with the desired axial impulse response. The resulting binary filters take the form of concentric transparent and opaque zones of equal area or equal width. Taking the axially superresolving filter as an example, we showed that the performance of the binary mask obtained by the 1D IFTA exceeds the performance of similar filters obtained with 1D ED algorithms if the resolution of the printing device is taken into account. In our experiment we did not optimize the IFTA for the number M of binary zones, the step of the parameter $e^{(k)}$ (i.e. $e^{(k+1)} - e^{(k)}$) or its initial value $e^{(1)}$. This suggests that further optimization is possible.

The 1D IFTA technique also exhibits a high SNR as far as focal plane impulse response is concerned. This allows us to believe that this algorithm could be a way for producing binary filters with controlled 3D impulse response around the focal point.

Acknowledgments

This work was supported by the Dirección General de Investigación Cientifica y Técnica (grant No. PB93-0354-C02-01), Ministerio de Educación y Ciencia, Spain, and by Komitet Badań Naukowych, Poland (project No. 8T11F 020 12).

References

[1] Ojeda-Castañeda, J., and Berriel-Valdós, L. R., 1988, *Optics Lett.*, **13,** 183.
[2] Ojeda-Castañeda, J., Tepichin, E., and Pons, A., 1988, *Appl. Optics*, **27**, 5140.
[3] Ojeda-Castañeda, J., Andrés, P., and Díaz, A., 1986, *Optics Lett.*, **11,** 487.
[4] Tsujiuchi, J., 1963, *Prog. Optics*, **2,** 131–180.
[5] Sheppard, C. J. R., and Hegedus, Z. S., 1988, *J. opt. Soc. Am.* A, **5,** 643.
[6] Martínez-Corral, M., Andrés, P., Ojeda-Castañeda, J., and Saavedra, G., 1995, *Optics Commun.*, **119,** 491.
[7] Martínez-Corral, M., Andrés, P., Silvestre, E., and Barreiro, J. C., 1995, *Second Iberoamerican Meeting on Optics*, Vol. 2730. (Bellingham, Washington: SPIE—The International Society for Optical Engineering).
[8] Engel, A., and Herziger, G., 1973, *Appl. Optics*, **12,** 471.
[9] Bryngdahl, O., Scheermesser, T., and Wyrowski, F., 1994, *Prog. Optics*, **33,** 389–463.
[10] Kowalczyk, M., Cichocki, T., Martínez-Corral, M., and Kober, V., 1995, *Pure appl. Optics*, **4,** 553.
[11] Kowalczyk, M., Cichocki, T., and Martínez-Corrall, M., 1995, *J. Soc. Inf. Display*, **3,** 67.
[12] Hegedus, Z. S., 1985, *Optica Acta*, **32,** 815.
[13] Kowalczyk, M., Martínez-Corral, M., Cichocki, T., and Andrés, P., 1995, *Optics Commun.*, **114,** 211.
[14] Rosen, J., and Yaariv, A., 1994, *Optics Lett.*, **19,** 843.
[15] Peter, T., Wyrowski, F., and Bryngdahl, O., 1993, *J. mod. optics*, **40,** 591.
[16] Martínez-Corral, M., Andrés, P., and Ojeda-Castañeda, J., 1994, *Appl. Optics*, **33,** 2223.
[17] Weissbach, S., and Wyrowski, F., 1992, *Appl. Optics*, **31,** 251.
[18] Fienup, J. R., 1980, *Opt. Engng.*, **19,** 297.
[19] Floyd, R. W., and Steinberg, L., 1976, *Proc. Soc. Inf. Display*, **17,** 75.
[20] Yzuel, M. J., Escalera, J. C., and Campos, J., 1990, *Appl. Optics*, **29,** 1631.